JOURNAL OF PROPULSION AND POWER
Vol. 11, No. 4, July–August 1995

Analysis of RDX Monopropellant Combustion with Two-Phase Subsurface Reactions

Yeong-Cherng Liau* and Vigor Yang†
Pennsylvania State University, University Park, Pennsylvania 16802

A comprehensive numerical analysis has been developed to study the key physicochemical processes involved in the self-sustained combustion of 1,3,5-trinitrohexahydro-s-triazine (RDX) monopropellant. The model takes into account detailed chemical kinetics and transport phenomena in the gas phase, and thermal decomposition and subsequent reactions in the condensed phase. The formation of gas bubbles in the subsurface layer due to molecular degradation and evaporation is also included to provide a complete simulation. Various important aspects of RDX burning characteristics are systematically examined over a broad range of pressure, with special attention given to the effect of the subsurface two-phase flow on propellant deflagration. Good agreement between calculated and measured burning rates as well as their pressure and temperature sensitivities is achieved. Results of species concentrations reveal a multistage reaction mechanism in the gas phase. The temperature profile, however, exhibits a monotonic increase from the surface to the final flame zone. No evidence is obtained of the existence of a temperature plateau in the dark zone, consistent with some experimental observations of self-deflagrating RDX flames using microthermocouple techniques. Further investigation into the gas-phase chemical kinetics is required to establish a unified understanding of RDX combustion under different operating conditions.

Nomenclature

A = cross-sectional area of propellant sample
A_g = fractional cross-sectional area consisting of gas bubbles in two-phase region
A_j = pre-exponential factor of rate constant of reaction j
A_s = interface area between bubbles and liquid per unit volume
B_j = temperature exponent in rate constant of reaction j
C_i = molar concentration of species i
c_{pi} = constant-pressure heat capacity of species i
E_j = activation energy of reaction j
e = internal energy
H_v = enthalpy of vaporization
h = enthalpy
h_c = heat-transfer coefficient
h_i = static enthalpy of species i
h_{fi}^0 = heat of formation of species i at standard condition
k_j = rate constant of reaction j
$\dot{m}''$ = mass flux
N = total number of species
N_R = total number of reactions
p = pressure
p_0 = pre-exponential factor of vapor pressure in Arrhenius form
q = heat release per unit mass
R_u = universal gas constant
T = temperature
s = sticking coefficient
t = time
u = bulk velocity
V_i = diffusion velocity of species i
W_i = molecular weight of species i
$\dot{w}_i$ = mass production rate of species i
$\dot{w}_{Rj}$ = mass production rate of reaction j
X_i = molar fraction of species i
x = spatial coordinate
Y_i = mass fraction of species i
λ = thermal conductivity
ρ = density
ϕ = void fraction
$\dot{\omega}$ = molar production rate

Subscripts

c = condensed phase
$c \rightarrow g$ = from condensed to gas phase
cond = condensation
eq = equilibrium condition
evap = evaporation
g = gas phase
s = propellant surface
v = vapor
0^+ = gas-phase side of propellant surface
0^- = condensed-phase side of propellant surface

Received May 20, 1995; revision received June 2, 1995; accepted for publication June 6, 1995.

*Graduate Student, Department of Mechanical Engineering.
†Professor, Department of Mechanical Engineering. Associate Fellow AIAA.

Introduction

CYCLO-TRIMETHYLENE-TRINITRAMINE (or hexahydro-1,3,5-trinitro-1,3,5-triazine) is an energetic compound that has been widely used as an oxidizer in composite propellants, producing high specific impulse, but little smoke, toxicity, and corrosion. This compound is given the acronym RDX since it was named "Royal Daughter's Explosive" by British chemists, while the term "hexogen" is commonly adopted in the Russian and French literature, owing to its molecular structure shown in Fig. 1. In spite of its broad applications, fundamental understanding of the detailed physicochemical processes involved in the combustion of RDX monopropellant remains limited. The major obstacle lies in the difficulties in conducting experimental and theoretical investigations into the combustion wave structures at scales sufficient to resolve the detailed chemical kinetic pathways and thermodynamic processes in the subsurface two-phase region as well as in the gas phase. The lack of reliable thermochemical properties of RDX and its associated pyrolysis and com-

Table 1 Thermal decomposition pathways of RDX

Proposed reactions	Remarks	Reference
RDX → 0.35CO + 0.55CO_2 + 0.62N_2 + 0.35N_2O + 1.9 NO + 0.19NO_2 + 1.95H_2O + 1.9HCN + 0.19HNCO	Exp. diag. using MP/TOFMS[a] p = 0.5 atm, self-sustained combustion No kinetic data reported	Korobeinichev et al.[5]
RDX → 0.31CO + 0.073CO_2 + 0.87N_2 + 0.58N_2O + 0.8NO + 0.95NO_2 + 1.05H_2O + 1.36HCN + 1.24CH_2O + 0.036H_2	Exp. diag. using MP/TQMS[b] p = 0.5 atm, laser-assisted combustion CO_2-laser heat flux: 100–200 W/cm^2 No kinetic data reported	Fetherolf and Litzinger[15]
RDX ⇌ RDXR + NO_2	Review of exp. work (1944–1983)	Schroeder[16–18]
RDX + NO_2 → mass 221[c] + HONO	Global decomposition rates reported	
RDX + NO_2 → RDXR + N_2O_4 or mass 206[c] + NO_3	No detailed reaction rates reported	
RDX + H_2CO → mass 223[c] + HCO		
RDX → RDXR + NO_2 → RDXRO + NO_2 → 2CH_2NNO_2 + H_2CN + NO_2	Theoretical analysis	Melius[8]
RDX → 3CH_2O + 3N_2O (water catalyzed)	Bond energy (potential) estimated using BAC-MP4[d] quantum chemical method	
CH_2NNO_2 → HCN + HONO	Kinetic data reported	
CH_2NNO_2 → H_2CN + NO_2		
RDX → RDXR + NO_2 → NO, OH, CN	Exp. diag. using TOFMS[a]	Beard[9]
RDX → a ring structure + HONO, O, NO, H_2O, H_2, HNO	X-ray and Nd/YAG laser-induced decomposition No kinetic data reported	Krause et al.[10]
RDX → 3CH_2NNO_2 (R1)	Exp. diag. using IRMPD[e] molecular beam/TOFMS[a]	Zhao et al.[7]
RDX → mass 176[c] + NO_2 (R2)	Pulse CO_2 laser, 6–20 J/cm^2 in 600 ns (equivalent heat flux = 10–33 MW/cm^2)	
CH_2NNO_2 → HCN + HONO (R3)	Branching ratios of R1/R2, R3/R4, and R5/R6 reported	
CH_2NNO_2 → N_2O + H_2CO (R4)	No detailed reaction rates reported	
Mass 176[c] + NO_2 → mass 129[c] + HONO (R5)	Exp. diag. using STMBMS/TOF[f] and DKIE[g] techniques	Behrens and Bulusu[11]
Mass 176[c] → mass 130[c] + NO_2 (R6)	Data obtained at very low heating rate (0.58 K/min) in solid phase	
RDX → OST + H_2O + NO + NO_2 (30%)	No kinetic data reported	
RDX → NO_2 + H_2CN + 2N_2O + 2CH_2O (10%)		
RDX + NO → ONDNTA → CH_2O + N_2O + others (35%)		
RDX → N_2O + CH_2O + NO_2 + NH_2CHO (25%) (catalyzed)		
RDX → RDXR + NO_2	CO_2 laser-induced pyrolysis/FTIR[h] technique	Wight and Botcher[12]
RDX → N_2O_4 + mass 130[c] or RDX + NO_2 → N_2O_4 + RDXR under high heating rate → NO, CO_2, N_2O, HCN, ...	Heating at the rates of 1.4–4.7 J/cm^2 No CH_2NNO_2 detected No kinetic data reported	Botcher and Wight[13]
RDX → 3CH_2O + 3N_2O	Exp. diag. using T-jump[i]/FTIR technique	Brill et al.[14]
RDX → 3HCN + 3NO_2 + 3H 5CH_2O + 7NO_2 → 7NO + 3CO + 2CO_2 + 5H_2O	Kinetic data adopted from literature and estimated by N_2O/NO_2 ratio	Lin et al.[19]

[a]Microprobe/time-of-flight mass spectrometry.
[b]Microprobve/triple-quadripole mass spectrometry.
[c]Molecular weight.
[d]Bond-additivity-corrected Møller–Plesset fourth-order perturbation theory.
[e]Infrared multiphoton dissociation.
[f]Simultaneous thermogravimetry modulated beam mass-spectrometry/time-of-flight velocity-spectra analysis.
[g]Deuterium kinetic isotope effect.
[h]FTIR.
[i]Temperature jump at a rate of 2000 K/s.

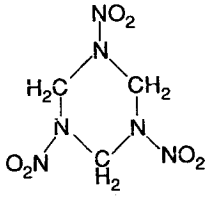

RDX

Fig. 1 Molecular structure of RDX compound.

bustion products poses another hurdle in improving the knowledge base. Comprehensive reviews of works conducted prior to 1984 are given by Boggs[1] and Fifer,[2] and the state of understanding up to 1990 is summarized by Alexander et al.[3]

Research on RDX and related nitramine-propellant combustion can be roughly categorized into three aspects: 1) thermal-decomposition mechanisms, 2) gas-phase reaction kinetics, and 3) modeling of overall combustion wave structures. The thermal decomposition mechanisms of RDX have been investigated for more than four decades, providing useful information about the initial chemical pathways and global reaction rates of the processes, RDX → products. Brill et al.[4] conducted a comprehensive review of this subject with emphasis placed on determination of the rate constants written in the Arrhenius form: $k = A \cdot \exp(-E_a/R_u T)$. More than 21 sets of data acquired during the period from 1949 to 1988 were compiled, covering a temperature range of 316–540 K in all three thermodynamic phases of solid, liquid, and gas. Results indicate that although reported pre-exponential factors A and activation energies E_a scatter substantially due to sample characteristics and experimental conditions, the discrepancies among the values of E_a are compensated for by the corresponding A. Consequently, the plot of E_a vs $\ln A$ produces an approximately straight line, and the overall rate constants are correlated well in terms of temperature, irrespective of the phase of the tested RDX sample. The rates of decomposition are roughly the same over the temperature range of measurement. Extrapolation of this result to another temperature range, however, may lead to erroneous prediction and must be exercised cautiously. Recently, more detailed decomposition pathways and associated intermediate species have been identified by means of advanced diagnostic and analytical techniques.[5–18] These results are summarized in Table 1. Unfortunately, the corresponding kinetic data and

thermochemical properties either remain unavailable or involve considerable uncertainties because of difficulties in acquiring the temporal and spatial characteristics of the intermediate species that are highly reactive and short lived.

Unlike research on thermal decomposition, only a few studies have been devoted to RDX gas-phase flame structures. Korobeinichev et al.[5] measured species-concentration profiles at 0.5 atm using a combined microprobe sampling and time-of-flight mass spectrometry (TOFMS) technique. The propellant sample was ignited by a hot wire and achieved self-sustained combustion without an external heat source. Measurements were performed only for the gas-phase region with resolution (over 100 μm) sufficient to resolve flame structures at low pressures, but not fine enough to analyze the surface-reaction zone. The microprobe TOFMS technique was later extended by Litzinger and co-workers[15,20] to include a triple-quadripole mass spectrometer (TQMS) capable of differentiating and quantifying species that could contribute to the same mass, such as N_2 and CO to mass 28 and N_2O and CO_2 to mass 44. The experiments were conducted in an argon environment over a pressure range of 0.1–3 atm, and a CO_2 laser was used to initiate and sustain combusion of the test samples at several heat fluxes ranging from 50 and 600 W/cm^2. Although the major species measured exhibit trends similar to those obtained by Korobeinichev et al.,[5] a direct comparison of these two sets of measurements is difficult. The application of the CO_2 laser results in two conspicuous phenomena: 1) higher NO_2 concentration at the surface (i.e., 5–18% in cases with laser heating, but only 1% in cases of self-sustained combustion) and 2) thicker flame zone (measured from surface to where HCN is mostly consumed). These effects usually become more profound as the laser heat flux increases.

Hanson-Parr and Parr[21] conducted pioneering measurements of temperature and species concentration profiles of RDX flames using nonintrusive planar laser-induced fluorescence (PLIF) and uv-visible absorption techniques. The samples were tested in air at 1 atm under a CO_2 laser heat flux of 600 W/cm^2. The reported temperature profile, obtained by assembling thermocouple measurements and rotational and vibrational spectra of NO and OH, exhibits the existence of a dark zone with a temperature plateau around 1700 K. The final flame temperature of 2600 K is substantially less than the adiabatic flame temperature (2923 K) predicted by the chemical equilibrium analysis due to heat loss to the ambient environment. The data also indicates that much of the depletion of NO occurs in the dark zone, not as expected in the secondary flame zone in which the reduction of NO to N_2 provides the major heat source for raising the flame temperature to its final value. In addition, the mole fraction of NO_2 is much higher than Korobeinichev's data. Recently, Zenin[22] conducted experimental investigations into self-deflagrating RDX flames, using a microthermocouple (MTC) technique at various pressures (1–90 atm). His results, however, do not reveal the existence of a temperature plateau in the dark zone even under atmospheric conditions. One factor contributing to this phenomenon is the severe heat loss to the surrounding gases, such that the maximum temperature in the measurement at 1 atm is only 1500 K. Boyer[23] employed the same MTC technique for self-sustained RDX combustion at 2 atm. The flame temperature increases monotonically from the surface and levels off at about 2600 K. No evidence is obtained of the existence of a temperature plateau in the dark zone.

The qualitative inconsistency among various measured temperature profiles may result from different experimental conditions (laser-assisted vs self-sustained combustion), sample compositions (pure vs waxed RDX), and diagnostic techniques (point vs line-of-sight measurements). The radial nonuniformity of flame structure also contributes to this discrepancy. A systematic investigation into the gas-phase processes, together with a careful calibration of the measurement technique, over a broad range of test conditions is definitely needed in order to establish a unified understanding of the phenomenon.

In regard to the theoretical modeling, most of the early studies employed global reaction schemes for gas-phase processes.[24] Almost no information was given about detailed chemical pathways and transport mechanisms. The first development of a comprehensive model was initiated by Ermolin et al.[6] in an effort to simulate experimentally measured species-concentration profiles. The model accommodates 23 species and 49 reactions in the gas phase, but requires the propellant surface conditions as input parameters in order to match experimental data. A substantial improvement was made by Melius[8] to relax this constraint. His formulation simultaneously takes into account the thermal decomposition of RDX and the ensuing chemical reactions to an extent that the key heat-release mechanisms can be identified. The thermochemical properties of giant molecules and related kinetic data were estimated using a quantum chemical method based on the BAC-MP4 (bound-additivity corrected Møller–Plesset fourth-order perturbation) scheme. In particular, a decomposition mechanism was postulated in accordance with the calculated bond dissociation energies. Because of its completeness, the model enables a systematic investigation into the detailed chemical processes involved in the gas-phase combustion. The model has been validated against the experimental data reported by Korobeinichev et al.[5] for $p = 0.5$ atm. Reasonable agreement was obtained in terms of the qualitative trend of species concentrations. Recently, Yetter et al.[25] refined Melius' model to include the submodels of reactions among the major intermediate products such as CH_2O, NO_2, N_2O, H_2, HCN, and NO. The kinetic parameters were also updated through flow-reactor experiments conducted at $550 < T < 1200$ K and $1 < p < 20$ atm, with residence times between 10–2000 ms. As will be shown later, both the Melius and Yetter models lead to a temperature profile that increases monotonically from the propellant surface to the final flame zone for the case of self-sustained combustion. The two-stage flame structure, as evidenced in Parr's measurement[21] under laser heat flux, was not observed.

Although the existence and importance of a molten foam layer at the surface of a deflagrating RDX propellant have long been acknowledged, very limited efforts have been made to simulate the detailed processes in this region because of the complexity involved. Margolis, Williams, Li, and co-workers[26–29] developed an analytical approach that takes into account the presence of gas bubbles and liquid droplets in the two-phase region by means of methods of matched asymptotic expansion. Two subregions are identified in the foam layer[26]: one, at higher liquid volume fractions, maintains evaporative equilibrium; whereas the other, at lower liquid volume fractions, exhibits nonequilibrium evaporation. Good agreement with measured burning rates and pressure sensitivity is achieved through small adjustments in overall chemical–kinetic parameters. However, since only global reactions are considered, the model provides limited information concerning the chemical processes.

The purpose of the present work is to establish a comprehensive framework for studying the key physicochemical processes involved in the combustion of RDX monopropellant. The model accommodates detailed chemical kinetics and transport phenomena in the gas phase, as well as thermal decomposition and subsequent reactions in the condensed phase. The formation of gas bubbles in the molten surface layer due to molecular degradation and thermodynamic phase transition is also included to provide a complete description. The model is capable of treating the entire combustion-wave structure, with instantaneous burning rate calculated as part of the solution. This article is organized as follows. First, a theoretical formulation of RDX combustion is established, followed by a brief discussion of the numerical technique used

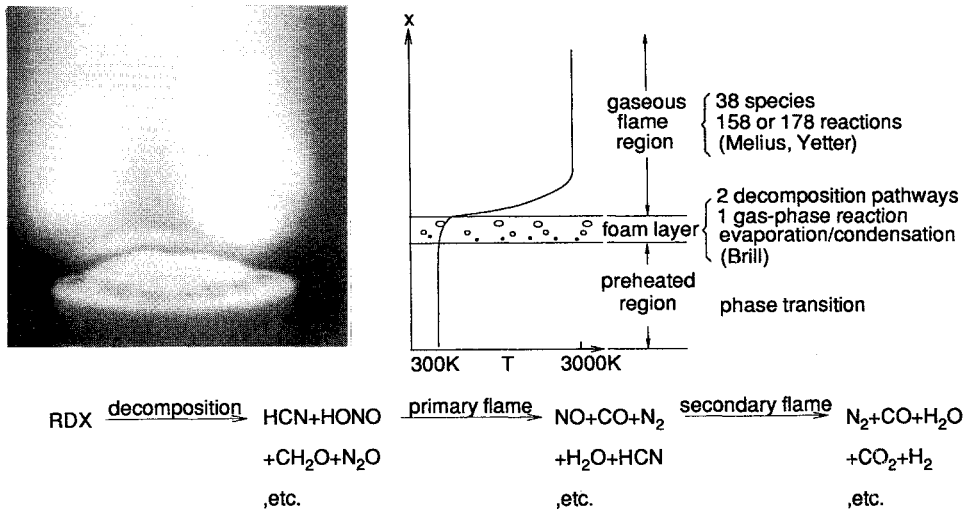

Fig. 2 Strand of RDX burning in a stagnant environment.

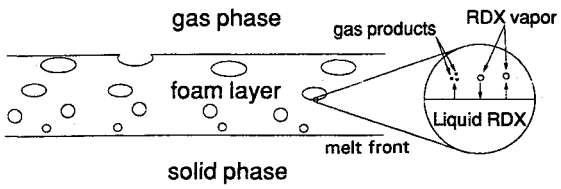

Fig. 3 Schematic diagram showing various regions in RDX combustion wave structure.

in this work. Various important aspects of RDX burning characteristics are examined over a broad range of pressure, with special attention given to the effect of the subsurface two-phase flow on propellant deflagration.

Theoretical Formulation

Figure 2 shows the physical model of concern, a strand of self-deflagrating RDX monopropellant in a stagnant environment. To facilitate analysis, the entire combustion-wave structure is conveniently segmented into three regions: 1) solid phase, 2) near-surface two phase, and 3) gas phase, as shown in Fig. 3. During burning, the propellant remains thermally stable in the solid phase until the temperature reaches the melting point at which thermodynamic phase transition occurs. Molecular degradation and evaporation of RDX then take place in the liquid layer, generating bubbles and forming a two-phase region. The propellant subsequently undergoes a sequence of rapid evaporation and decomposition in the near field immediately above the foam layer. Oxidation reactions continue to occur and to release an enormous amount of energy in the gas phase, with the final temperature reaching the adiabatic flame temperature. A brief summary of the theoretical formulation of physicochemical processes in various regions is given later. Detailed derivations can be found in Ref. 30.

Gas-Phase Processes

The analysis for the gas phase is based on the mass, energy, and species transport for a multicomponent chemically reacting system of N species, and accommodates finite rate chemical kinetics and variable thermophysical properties. If body forces, viscous dissipation, and radiation are ignored, the conservation equations for an isobaric flow can be written as follows:

Mass

$$\frac{\partial \rho}{\partial t} + \frac{\partial}{\partial x}(\rho u) = 0 \tag{1}$$

Species concentration

$$\frac{\partial(\rho Y_i)}{\partial t} + \frac{\partial[\rho(u + V_i)Y_i]}{\partial x} = \dot{w}_i \qquad (i = 1, 2, \ldots, N) \tag{2}$$

Energy

$$\frac{\partial(\rho e)}{\partial t} + \frac{\partial(\rho u h)}{\partial x} = \frac{\partial}{\partial x}\left(\lambda \frac{\partial T}{\partial x} - \sum_{i=1}^{N} \rho Y_i V_i h_i\right) \tag{3}$$

where the subscript i denotes the ith species. The specific enthalpy of a mixture is the mass-weighted sum of the species enthalpy h_i

$$h = \sum_{i=1}^{N} h_i Y_i \quad \text{and} \quad h_i = \int_{T_{\text{ref}}}^{T} c_{p_i}\, \mathrm{d}T + h_{f_i}^0 \tag{4}$$

where $h_{f_i}^0$ is the enthalpy of formation of species i. Standard notations in thermodynamics and fluid mechanics are used in Eqs. (1–4), including ρ for density, u for bulk velocity, V_i for mass diffusion velocity, Y_i for mass fraction of species i, and $\dot{w}_i$ for rate of production of species i. Consequently, the specific internal energy becomes

$$e = h - (p/\rho) \tag{5}$$

The mass diffusion velocity V_i consists of contributions from both concentration and temperature gradients

$$V_i = -D_i \frac{1}{X_i}\frac{\partial X_i}{\partial x} + D_i \frac{D_{T_i}}{X_i}\frac{1}{T}\frac{\partial T}{\partial x} \tag{6}$$

where D_i denotes the effective mass-diffusion coefficient for species i, and D_{T_i} the thermal diffusion ratio. Finally, the equation of state for a multicomponent system is derived to close the formulation.

$$p = \rho R_u T \sum_{i=1}^{N} \frac{Y_i}{W_i} \tag{7}$$

where R_u is the universal gas constant and W_i the molecular weight of species i.

Gas-Phase Chemical Kinetics

For a set of N_R elementary reactions involving N species, the reaction equations can be written in the following general form:

$$\sum_{i=1}^{N} \nu'_{ij} M_i \underset{k_{bj}}{\overset{k_{fj}}{\rightleftharpoons}} \sum_{i=1}^{N} \nu''_{ij} M_i, \qquad j = 1, 2, \ldots, N_R \tag{8}$$

where ν'_{ij} and ν''_{ij} are the stoichiometric coefficients for species i appearing as a reactant in the jth forward and backward reactions, respectively, and M_i is the chemical symbol for species i. The reaction rate constant k_j (either k_{fj} or k_{bj}) is given empirically by the Arrhenius expression

$$k_j = A_j T^{B_j} \exp(-E_j/R_u T) \tag{9}$$

where E_j represents activation energy, and A_j and B_j are empirical constants. The rate of change of molar concentration of species i by reaction j is

$$\dot{C}_{ij} = (\nu'_{ij} - \nu''_{ij}) \left(k_{fj} \prod_{i=1}^{N} C_i^{\nu'_{ij}} - k_{bj} \prod_{i=1}^{N} C_i^{\nu''_{ij}} \right) \tag{10}$$

The total rate of change of species i in Eq. (2) is then obtained by summing up the changes due to all reactions:

$$\dot{w}_i = W_i \sum_{j=1}^{N_R} \dot{C}_{ij} \tag{11}$$

It should be noted that the expression for chemical reaction rate [Eq. (10)], is valid strictly for elementary reactions. If a global kinetics scheme is used, the exponents for molar concentrations may differ from their stoichiometric coefficients in order to match experimental data.

The reaction mechanisms proposed by Melius[8] and Yetter et al.[25] are employed to model the gas-phase chemical kinetics. Melius' scheme consists of 38 species and 158 reactions, being derived by extending a generalized hydrocarbon/air flame model of Miller and co-workers.[31-33] The mechanisms include the oxidation of HCN, the conversion of NH_i species to NO and N_2, and the flame chemistry of C_2N_2/NO_2. Additional reactions are considered to treat the decomposition of RDX and the subsequent reactions of intermediate species. The thermochemical data of species not in the literature was calculated using the BAC-MP4 quantum chemical method.

Yetter et al.[25] adopted the same initial decomposition scheme for RDX propellant as that proposed by Melius, but used a modified set of subsequent reactions. Their model is based on a hierarchical approach for collecting kinetic data and the specific chemical submodels that are required to form the gas-phase combustion mechanism. In particular, three kinetic submodels of increasing complexity (N_2O decomposition, H_2/NO_2 reaction, and CH_4/N_2O reaction) are established using the results from kinetic experiments over a broad range of temperature and pressure. The overall scheme required 38 species and 178 reactions. Although the trends of the Melius and Yetter models are consistent in terms of predicted temperature and species concentration profiles, significant differences are observed in many of the pathways of secondary reactants.

Subsurface Processes

For convenience, the foam layer and condensed phase underneath the propellant burning surface are treated together and referred to as the subsurface region. The physicochemical processes in this region are extremely complex, involving an array of intricacies such as thermal decomposition, evaporation, bubble formation, gas-phase reactions in bubbles, interfacial transport of mass and energy between gas and condensed phases, etc. A two-phase fluid dynamic model using a spatial-averaging technique is employed to formulate these complicated phenomena. The analysis is based on the integral form of conservation laws for control volumes occupied separately by the gas-bubble and condensed phases. In establishing the gas-phase formulation, the Dupuit–Forchheimer assumption, which permits the fractional-volume voidage definition of porosity ϕ to be extended to a fractional-area voidage definition[34] is employed, giving

$$A_g = \phi A \tag{12}$$

where A is the cross-sectional area of the propellant sample, and A_g the fractional cross-sectional area consisting of gas bubbles. This assumption is valid so long as there are numerous gas bubbles distributed randomly, as is the present case. The one-dimensional conservation equations for the gas phase take the following form:

Mass

$$\frac{\partial(\phi\rho_g)}{\partial t} + \frac{\partial}{\partial x}(\phi\rho_g u_g) = \dot{w}_{c\to g} \tag{13}$$

Species concentration

$$\frac{\partial(\phi\rho_g Y_{g_i})}{\partial t} + \frac{\partial[\phi\rho_g(u_g + V_{g_i})Y_{g_i}]}{\partial x} = \dot{w}_{g_i} \qquad (i = 1, 2, \ldots, N_g) \tag{14}$$

Energy

$$\frac{\partial(\phi\rho_g e_g)}{\partial t} + \frac{\partial(\phi\rho_g u_g h_g)}{\partial x} = \frac{\partial}{\partial x}\left(\phi\lambda_g \frac{\partial T_g}{\partial x} - \phi \sum_{i=1}^{N_g} \rho_g Y_{g_i} V_{g_i} h_{g_i} \right) + \dot{w}_{c\to g} q_{c\to g} + A_s h_c (T_c - T_g) \tag{15}$$

where subscripts g and c denote the gas-bubble and condensed phases, respectively. The specific surface area A_s is defined as the interfacial area between bubbles and liquid per unit volume. The source term $\dot{w}_{c\to g}$ represents the rate of mass conversion from liquid to gas, $\dot{w}_g$ the rate of production of species i, and $\dot{w}_{c\to g} q_{c\to g}$ and $A_s h_c (T_c - T_g)$ the interphase energy transport through mass conversion and heat transfer, respectively.

Following the same procedure leading to Eqs. (13–15), the conservation equations for the condensed phase can be written as follows:

Mass

$$\frac{\partial[(1-\phi)\rho_c]}{\partial t} + \frac{\partial}{\partial x}[(1-\phi)\rho_c u_c] = -\dot{w}_{c\to g} \tag{16}$$

Species concentration

$$\frac{\partial[(1-\phi)\rho_c Y_{c_i}]}{\partial t} + \frac{\partial[(1-\phi)\rho_c(u_c + V_{c_i})Y_{c_i}]}{\partial x} = \dot{w}_{c_i} \qquad (i = 1, 2, \ldots, N_c) \tag{17}$$

Energy

$$\frac{\partial[(1-\phi)\rho_c e_c]}{\partial t} + \frac{\partial[(1-\phi)\rho_c u_c h_c]}{\partial x} = \frac{\partial}{\partial x}\left[(1-\phi)\lambda_c \frac{\partial T_c}{\partial x} - (1-\phi) \sum_{i=1}^{N_c} \rho_c Y_{c_i} V_{c_i} h_{c_i} \right] - \dot{w}_{c\to g} q_{c\to g} - A_s h_c (T_c - T_g) \tag{18}$$

It is worth noting that the mass diffusion velocities in the subsurface region V_{gi} and V_{ci} are usually quite small compared to their convective counterparts, and can be safely ignored to simplify numerical calculations.

Subsurface Chemical Kinetics and Phase Transition

Thermal decomposition and its ensuing reactions in the subsurface region have been investigated by many researchers,[9-14] as summarized in Table 1. Since these processes are extremely complicated and contain many uncertainties, a thorough consideration of all physico- and chemical mechanisms involved does not appear feasible. A reduced global kinetics model of Brill et al.,[14] which is derived from a well-calibrated temperature-jump/Fourier transform infrared (T-jump/FTIR) spectroscopy experiment, is therefore adopted here. This model is a viable alternative, providing reasonably accurate information concerning the major chemical pathways. The scheme first assumes two degradation reactions in the condensed phase:

$$\mathrm{RDX}_{(c)} \xrightarrow{k_1} 3\mathrm{CH_2O} + 3\mathrm{N_2O} \tag{R1}$$

$$\mathrm{RDX}_{(c)} \xrightarrow{k_2} 3\mathrm{HCN} + \tfrac{3}{2}\mathrm{NO} + \tfrac{3}{2}\mathrm{NO_2} + \tfrac{3}{2}\mathrm{H_2O} \tag{R2}$$

Reaction R1 is exothermic and is favored at low heating-rate conditions. The second reaction, R2, initiated by N—NO_2 bond cleavage, is endothermic and prevails at high heating rates. The net heat released from (R1) and (R2) is experimentally observed to be small.[14] Subsequent reactions among the products of (R1) and (R2) may occur and provide the thermal energy to sustain pyrolysis. Brill[35] examined several plausible secondary reactions (such as $CH_2O + NO_2$, $CH_2O + N_2O$, and $HCN + NO_2$) and their corresponding reaction rates. Results indicate that the following reaction

$$\mathrm{NO_2} + \mathrm{CH_2O} \xrightarrow{k_3} \mathrm{NO} + \mathrm{CO} + \mathrm{H_2O} \tag{R3}$$

is probably the most important secondary reaction in the condensed-phase environment if it indeed does occur. Furthermore, the concentrations of NO_2 and CH_2O decrease while NO, CO, and H_2O increase at the later stage of the T-jump/FTIR experiments. The concentration ratio of N_2O/NO_2 as a function of temperature has been measured and was used to determine the branching ratio of (R1) and (R2).[14,36] The resulting rate constants and mass (or molar) consumption rates can be written as

$$k_1 = 6 \times 10^{13} \exp\left(-36 \frac{\text{kcal}}{\text{mol}} \Big/ R_u T\right), \ \text{s}^{-1}$$
$$\dot{w}_{R1} = (1 - \phi)\rho_c k_1 \tag{19}$$

$$k_2 = 16 \times 10^{16} \exp\left(-45 \frac{\text{kcal}}{\text{mol}} \Big/ R_u T\right), \ \text{s}^{-1}$$
$$\dot{w}_{R2} = (1 - \phi)\rho_c k_2 \tag{20}$$

$$k_3 = 802 \times T^{2.77} \exp\left(-13.73 \frac{\text{kcal}}{\text{mol}} \Big/ R_u T\right), \ \frac{\text{cm}^3}{\text{mol}\cdot\text{s}}$$
$$\dot{\omega}_{R3} = \phi k_3 \frac{\rho_g Y_{\mathrm{CH_2O}}}{W_{\mathrm{CH_2O}}} \frac{\rho_g Y_{\mathrm{NO_2}}}{W_{\mathrm{NO_2}}} \tag{21}$$

Note that the rate constants in Eqs. (19) and (20) are adopted from Ref. 36, while those in Eq. (21) from Ref. 19.

In addition to thermal decomposition and subsequent reactions, (R1–R3), thermodynamic phase transition from liquid to vapor RDX is considered to provide a complete description of the mass conversion process:

$$\mathrm{RDX}_{(c)} \rightleftharpoons \mathrm{RDX}_{(g)} \tag{R4}$$

The process consists of both evaporation and condensation, and can be modeled using gas-kinetic theory. The condensation mass flux can be characterized in terms of the rate at which vapor molecules collide and stick to the interface:

$$\dot{m}''_{\text{cond}} = s\dot{n}''W \tag{22}$$

The sticking coefficient s is treated as an empirical constant that depends on local conditions at the interface, usually having a value close to unity. The molar flux of vapor molecules hitting the surface $\dot{n}''$ equals the product of the molar concentration and average molecular velocity component normal to the interface. For an ideal gas with the Maxwell distribution of molecular speed, the condensation mass flux takes the form

$$\dot{m}''_{\text{cond}} = s(\tfrac{1}{4}\sqrt{8R_u T/\pi W})(pW/R_u T)X \tag{23}$$

If thermodynamic phase equilibrium is achieved, the evaporation process proceeds at the same rate as the condensation process

$$\dot{m}''_{\text{evap}} = \dot{m}''_{\text{cond}} = s(\tfrac{1}{4}\sqrt{8R_u T/\pi W})(pW/R_u T)(p_{v,\text{eq}}/\text{p}) \tag{24}$$

where the equilibrium vapor pressure $p_{v,\text{eq}}$ can be approximated by the Clausius–Clapeyron equation

$$p_{v,\text{eq}} = p_0 \exp[-(H_v/R_u T)] \tag{25}$$

At nonequilibrium conditions, the net evaporation rate is taken to be the difference between the evaporation and condensation rate, giving

$$\dot{m}''_{\text{net}} = s(\tfrac{1}{4}\sqrt{8R_u T/\pi W})(pW/R_u T)[(p_{v,\text{eq}}/p) - X] \tag{26}$$

Thus, the specific mass conversion rate due to evaporation becomes

$$\dot{w}_{R4} = A_s \dot{m}''_{\text{net}} \tag{27}$$

The specific surface area A_s is a function of void fraction and number density of the bubbles and is derived as follows:

$$A_s = (36\pi n)^{1/3}\phi^{2/3}, \quad \phi < 1/2$$
$$\text{or} \quad (36\pi n)^{1/3}(1 - \phi)^{2/3}, \quad \phi > 1/2 \tag{28}$$

where n is the number density of bubbles to be determined empirically.

Boundary Conditions

The physical processes in the gas phase and foam layer must be matched at the propellant surface to provide the boundary conditions for each region. This procedure requires balances of mass and energy, and eventually determines propellant surface conditions and burning rate. With the application of conservation laws to the propellant surface, the matching conditions are expressed as follows:

Mass

$$[(1 - \phi)\rho_c u_c + \phi\rho_g u_g]_{0^-} = (\rho u)_{0^+} \tag{29}$$

Species concentration

$$[(1 - \phi)\rho_c(u_c + V_{c_i})Y_{c_i} + \phi\rho_g(u_g + V_{g_i})Y_{g_i}]_{0^-}$$
$$= [\rho(u + V_i)Y_i]_{0^+} \tag{30}$$

Energy

$$\left[(1-\phi)\lambda_c \frac{dT_c}{dx} - \sum_{i=1}^{N_c}(1-\phi)\rho_c(u_c+V_{c_i})Y_{c_i}h_{c_i}\right]_{0^-} + \left[\phi\lambda_g \frac{dT_g}{dx} - \sum_{i=1}^{N_g}\phi\rho_g(u_g+V_{g_i})Y_{g_i}h_{g_i}\right]_{0^-} = \left[\lambda \frac{dT}{dx} - \sum_{i=1}^{N}\rho(u+V_i)Y_ih_i\right]_{0^+} \quad (31)$$

where subscripts 0^+ and 0^- represent conditions at the interface on the gas and subsurface sides, respectively. A distinct phase transition from liquid to vapor RDX is assumed to prevail at the interface, giving

$$[(1-\phi)\rho_c u_c]_{0^-} = \dot{m}''_{\text{net}} \quad (32)$$

Equations (29–32), coupled with the assumption that $\rho_g u_g = \rho_c u_c$ and $T_g = T_c$ in the condensed phase,[26] are sufficient to solve the set of unknowns (u, T_s, ϕ, Y_i) at the propellant surface.

The far-field conditions for the gas phase require that the gradients of flow properties be zero at $x = \infty$:

$$\frac{\partial\rho}{\partial x} = \frac{\partial u}{\partial x} = \frac{\partial Y_i}{\partial x} = \frac{\partial T}{\partial x} = 0 \quad \text{at} \quad x = \infty \quad (33)$$

The conditions at the cold boundary for the condensed phase ($x = -\infty$) are

$$T_g = T_c = T_i \quad \text{and} \quad \phi = 0 \quad \text{at} \quad x = -\infty \quad (34)$$

where T_i is the conditioned initial temperature of the propellant. Finally, the phase transition from solid to liquid at the melting point ($T = 478$ K) is considered part of the subsurface process.

Numerical Method

The theoretical formulation established in the preceding section results in two types of computational difficulties: 1) stiffness due to the wide variety of time and length scales associated with chemical reactions and transport processes, and 2) complexity arising from the entangled matching conditions at the propellant surface. The stiffness problem of the gas-phase processes can be effectively circumvented by using a combined Newton-iteration and time-integration scheme originally developed by Kee et al.[37] The Newton method functions efficiently for steady-state solutions, but may fail to converge unless a reasonable initial guess is provided. Conversely, the time-integration technique is more robust, but less efficient. To optimize the benefits of these two algorithms, calculations usually start with the Newton method, and then switch to the integration scheme when the iteration fails to converge. After another trial solution is obtained with several time-marching steps, the Newton method is resumed to gain efficiency. An adaptive-grid system is employed to further improve the convergence rate, while simultaneously acquiring the spatial resolution of the rapidly varying flow properties in the flame zone.

The overall calculation proceeds according to a double-iteration procedure, with the propellant surface temperature T_s and burning rate r_b treated as the eigenvalues of the analysis. The inner loop is used to adjust T_s and the outer loop to correct r_b. For a given initial guess of T_s and r_b, the conservation equations for the subsurface region are first solved. The resulting species concentrations at the surface are used to determine the boundary conditions for the gas phase through the interfacial matching conditions. The next step involves integration of the gas-phase conservation equations to provide the the temperature and species-concentration profiles. The mass-evaporation Eq. (32) is then employed to check the convergence of T_s. If not successful, another inner iteration is repeated using an updated value of T_s. The outer iteration follows the same procedure as the inner loop except that r_b is used as the eigenvalue to check the interfacial energy continuity, Eq. (31). Since only the burning rate and surface temperature, but not interfacial species concentrations, are involved in the iterative procedure, the present algorithm performs quite well and significantly reduces the computational burden.

Discussion of Results

A series of calculations were carried out to study the RDX combustion behavior over a broad range of pressure and initial temperature. Various important burning characteristics are investigated systematically, with emphasis placed on the detailed flame structure and the effect of the subsurface two-phase layer on propellant deflagration.

Figure 4 shows the temperature distributions at several pressures. The gas-phase chemical kinetics are based on the model of Yetter et al.,[25] and the thermophysical properties of RDX are obtained from Refs. 26 and 38. The temperature increases monotonically from its initial condition of 293 K, and levels off at a value intimately close to the prediction by the chemical equilibrium analysis. The final flame temperature increases with increasing pressure, whereas the flame standoff distance exhibits an opposite trend owing to enhanced chemical-reaction rates at high pressures. No evidence is obtained of the existence of a temperature plateau in the dark zone regardless of pressure, which is consistent with the experimental observation of self-sustained RDX combustion.[23] Figure 5 shows the burning rate as a function of

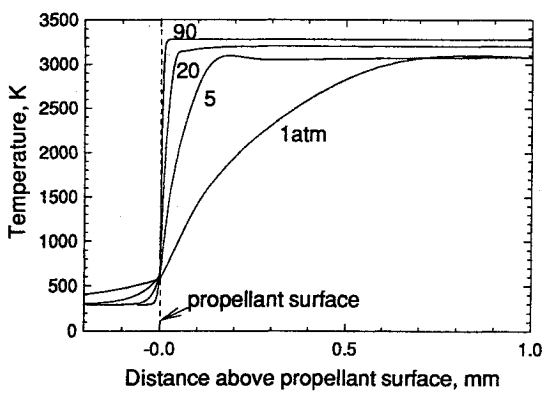

Fig. 4 Temperature profiles of self-sustained RDX combustion at various pressures.

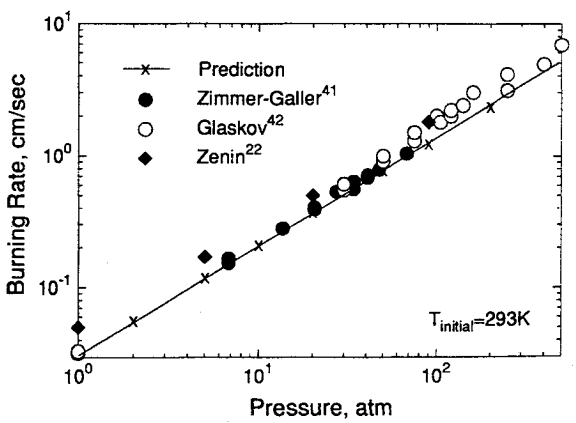

Fig. 5 Effect of pressure on strand burning rate of RDX monopropellant.

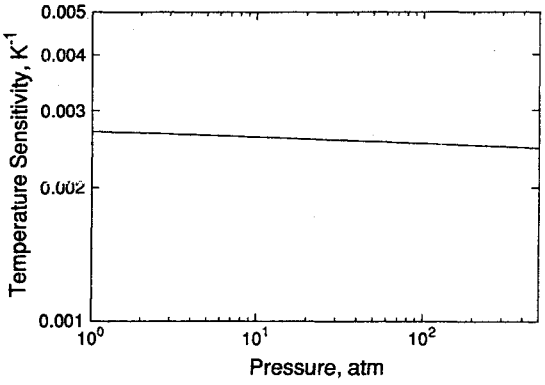

Fig. 6 Temperature sensitivity of RDX burning rate.

pressure. Good agreement between predictions and measurements is obtained. The pressure exponent n in the burning-rate law[39]

$$r_b = ap^n \tag{35}$$

is about 0.83, with the pre-exponential factor a equal to 0.3 for $T_i = 293$ K. The increased burning rate with pressure is attributed mainly to fast gas-phase exothermic reactions at high pressures and their influence on heat transfer to the condensed phase. The temperature sensitivity of burning rate defined in Eq. (36) is also examined, giving the result shown in Fig. 6:

$$\sigma_p = \left[\frac{(\partial r_b)/r_b}{\partial T_i}\right]_p = \left[\frac{\partial(\ln r_b)}{\partial T_i}\right]_p \tag{36}$$

The predicted σ_p is around 0.0028 K^{-1} at 1 atm, and decreases slightly with increasing pressure. At elevated pressures, the heat feedback from the gas to the condensed phase is higher and, as a consequence, the effect of initial temperature on the interfacial energy balance (which determines r_b), becomes less important.

The calculated species-concentration profiles are validated against experimental data[5] obtained by means of a time-of-flight mass spectrometry technique at 0.5 atm,[5] as shown in Fig. 7. Good agreement is obtained except for the region next to the surface. The discrepancy may arise from the ambiguity in determining the location of the propellant surface in experiments. The measured result indicates that RDX is completely consumed at the surface. The present analysis, however, predicts that an appreciable amount of RDX still exists at the surface since only limited RDX decomposition occurs in the subsurface region. If the spatial distribution of the calculated data is artificially shifted upward to the location where NO and HCN attain their peak values, then the prediction would match the measurement much better. The species-concentration profiles reveal a two-stage reaction mechanism. In the first stage, RDX decomposes to H_2O, NO, HCN, N_2, and CO, among other species. The second stage involves removal of HCN and NO and generation of the final products such as N_2, CO, and H_2.

Figures 8 and 9 present detailed distributions of temperature and major species concentrations in both the gas-phase and subsurface regions at 1 atm. The general trend is similar to that at 0.5 atm, but with a shorter flame standoff distance. The small hump in the temperature profile is thought to be associated with water dissociation at high temperature. In spite of the monotonicity of the temperature field, a multistage chemical pathway is clearly identified in the species-concentration profiles, as in the case of 0.5 atm. The overall reaction mechanisms globally consist of three steps: 1) decomposition of RDX to CH_2O, HCN, NO_2, etc., near the

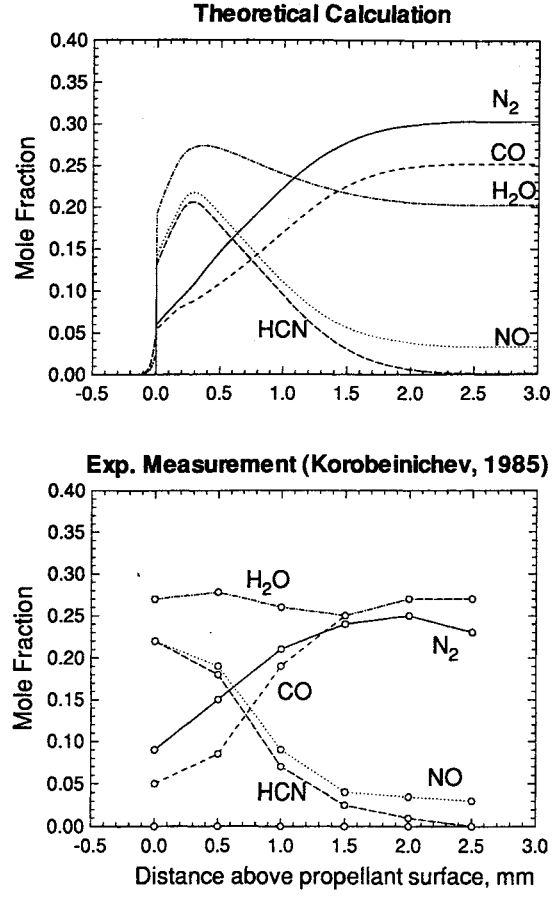

Fig. 7 Distributions of major species concentrations of self-sustained RDX combustion at 0.5 atm.

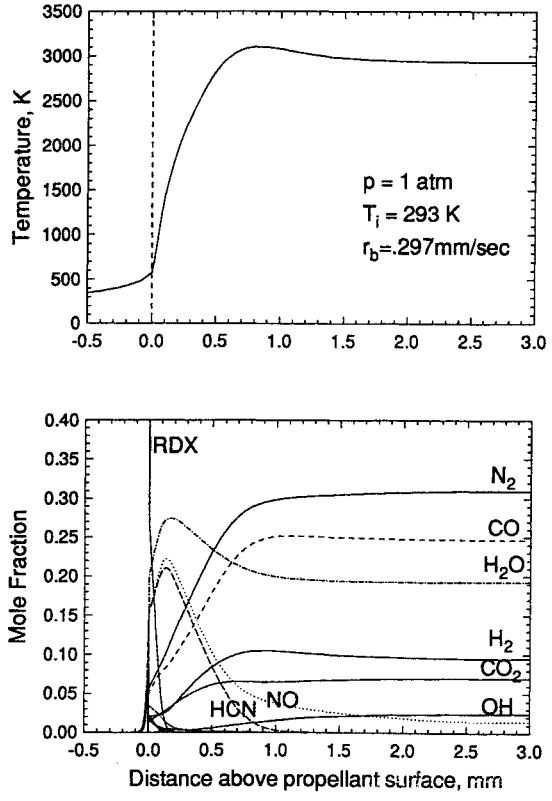

Fig. 8 Distributions of temperature and major species concentrations of self-sustained RDX combustion at 1 atm.

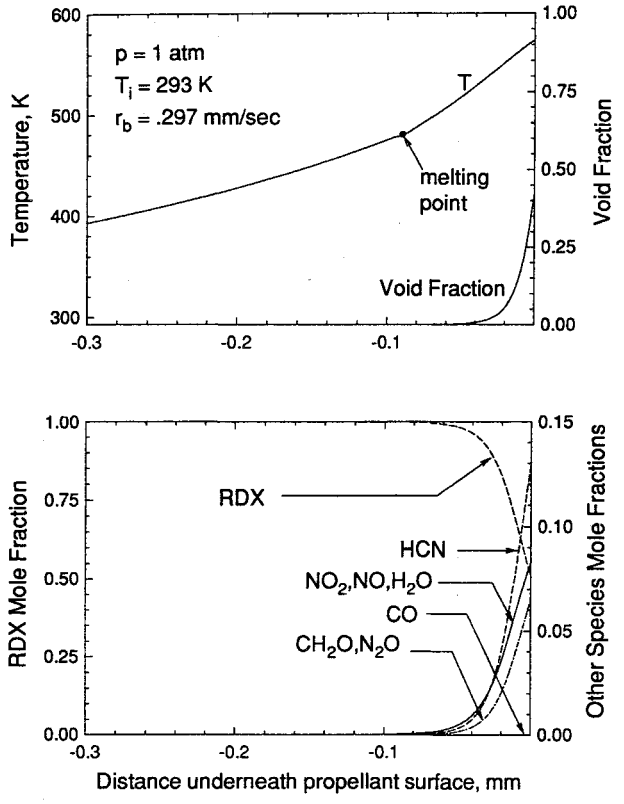

Fig. 9 Close-up view of temperature and species-concentration profiles in subsurface region at 1 atm.

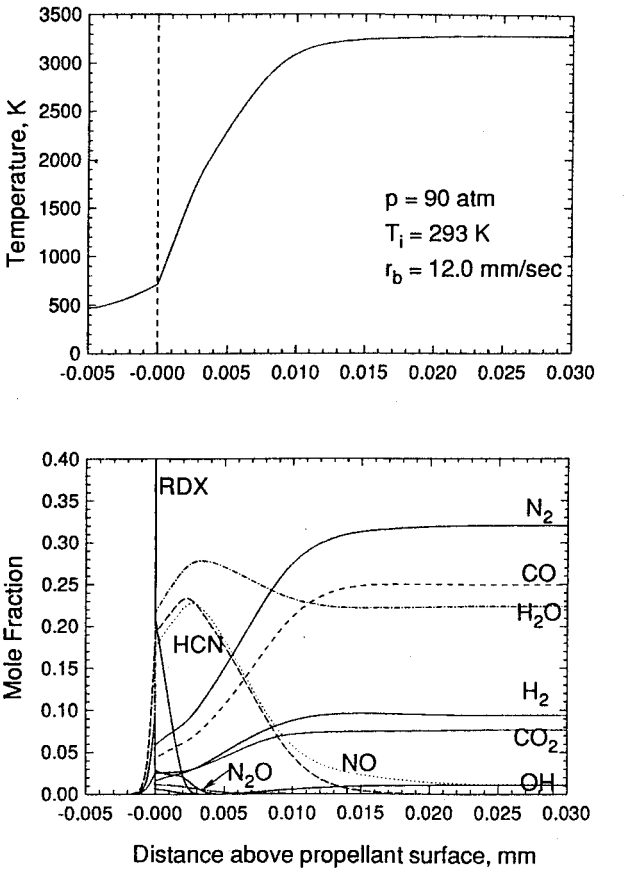

Fig. 10 Distributions of temperature and major species concentrations of self-sustained RDX combustion at 90 atm.

surface, 2) first-stage oxidization that includes formation of NO and H_2O as well as removal of NO_2, and 3) second-stage oxidization that includes conversion of HCN and NO to the final products such as CO, N_2, and H_2. It is worth noting that the highly exothermic reductions of HCN and NO usually occur at elevated temperature ($T \approx 2000$ K), owing to the large activation energies required to initiate these reactions, that provide the major heat source for raising the flame temperature to its final adiabatic value. The calculated molar fractions of the final product species are quite consistent with the chemical-equilibrium predictions, with the deviation being less than 2%.

The distribution of void fraction in the subsurface region shown in Fig. 9 indicates that as a result of RDX evaporation and decomposition, the gas bubbles occupy 45% of the volume at the surface. Within the temperature range in the two-phase layer, the endothermic decomposition of RDX, (R2), overrides the exothermic decomposition, (R1), and consequently gives rise to a higher mole fraction of HCN compared with CH_2O and N_2O. Furthermore, the reaction of NO_2 and CH_2O in gas bubbles, (R3), is almost negligible due to low mass concentrations and temperature.

The combustion wave structure at 90 atm is shown in Figs. 10 and 11, exhibiting a close similarity to that at 1 atm. The major difference lies in a smaller void fraction (about 35% at the surface), because high pressure tends to retard the RDX evaporation that dominates the gasification process in the two-phase layer. In addition, the endothermic decomposition, (R2), appears more profound as evidenced by the large ratio of HCN to CH_2O mole fraction. This can be attributed to the higher surface temperature and heat transfer into the condensed phase. The foam layer also becomes much thinner, and almost 50% of RDX is decomposed underneath the surface.

Figures 12 and 13 show the effect of pressure on molten-layer thickness and propellant surface behavior, respectively. The closed symbols denote experimental data from the mi-

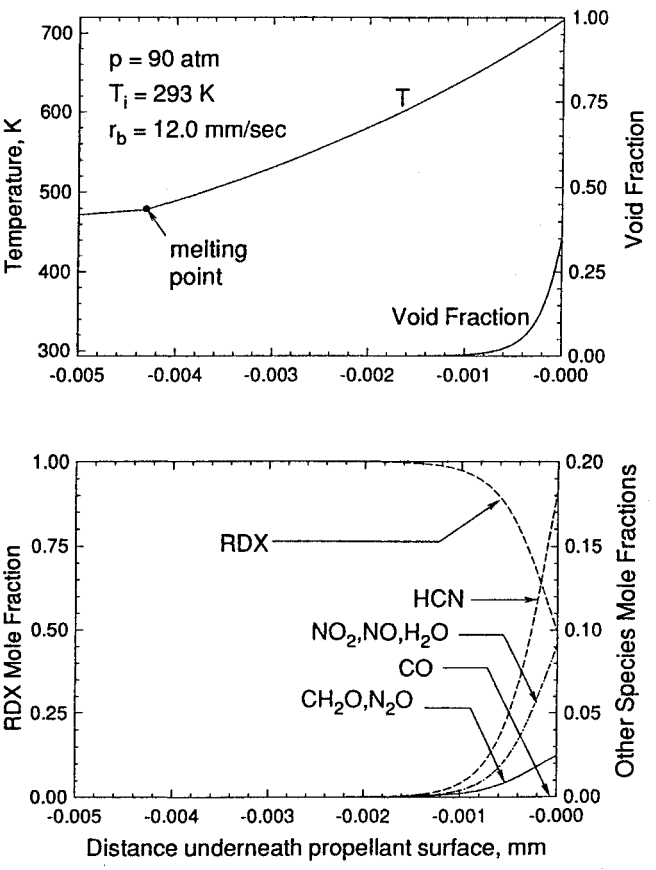

Fig. 11 Close-up view of temperature and species-concentration profiles in subsurface region at 90 atm.

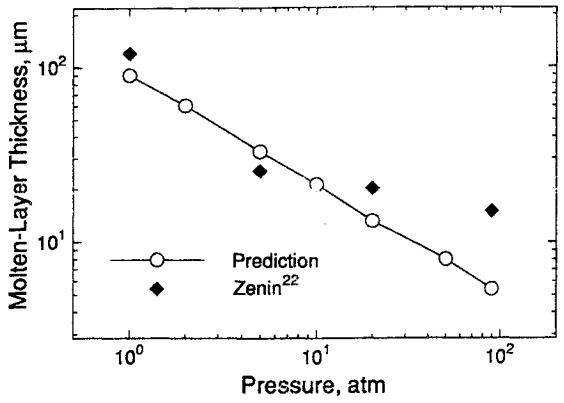

Fig. 12 Effect of pressure on molten-layer thickness.

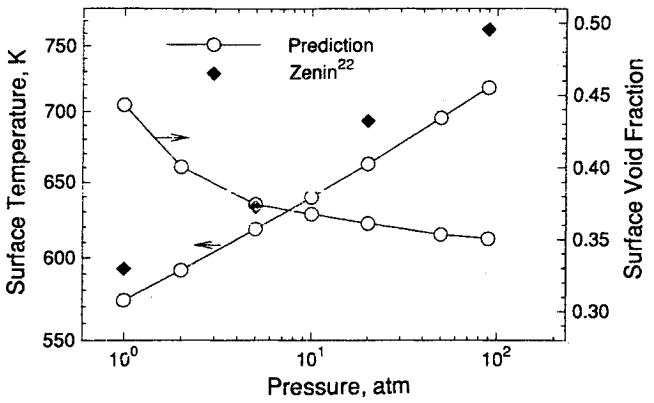

Fig. 13 Effect of pressure on surface temperature and void fraction.

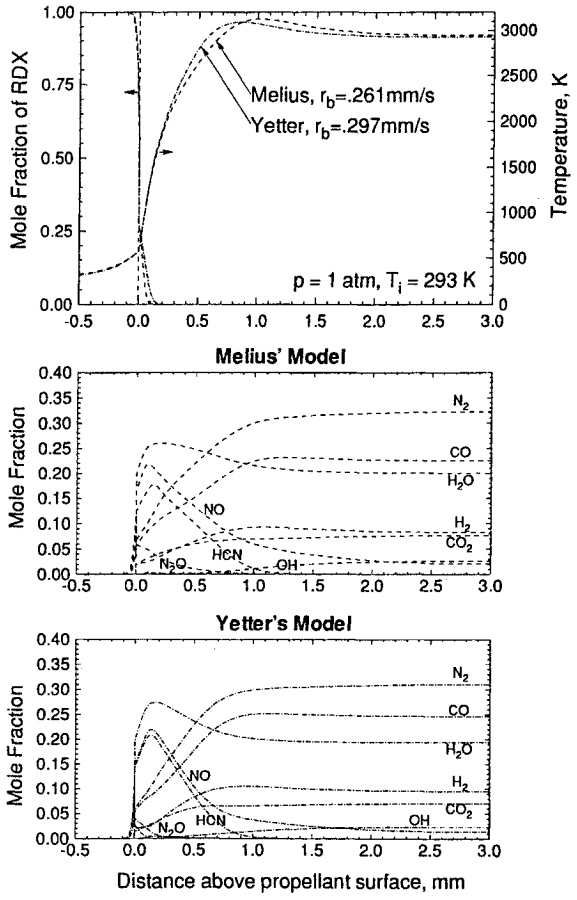

Fig. 14 Distributions of temperature and species concentrations predicted using Melius and Yetter chemical kinetics models at 1 atm.

crothermocouple temperature measurement.[22] The surface temperature increases with increasing pressure, but an opposite trend is observed for void fraction and molten-layer thickness. The condensed-phase process becomes less important as the ambient pressure increases, with the gas-phase reactions playing a more important role.

An important issue in the present analysis of RDX combustion is that the calculated gas-phase temperature does not reveal a plateau in the dark zone. This result, although consistent with measurements of self-sustained RDX deflagration,[22,23] appears to be in conflict with the findings from laser-assisted combustion experiments in which a temperature plateau at 1700 K is observed. In an effort to search for plausible explanations for this qualitative discrepancy, the original chemical kinetics scheme developed by Melius[8] is implemented in the gas-phase analysis. Figure 14 compares the Yetter[25] and Melius[8] models in terms of temperature and species-concentration distributions at 1 atm. Both schemes yield similar trends, but neither exhibit a two-stage structure in temperature. Yetter's model leads to a steeper temperature profile near the surface, and consequently a slightly higher burning rate. Recently, Li and Williams[40] proposed a chemical kinetics scheme for the primary flame of RDX deflagration, including a major decomposition channel not included in the schemes of Melius and Yetter. The model takes into account the concerted symmetric triple fission of RDX to produce three H_2CNNO_2 fragments,[7] which subsequently dissociate to HCN, HONO, CH_2O, and N_2O. When the scheme is used alone in the present analysis for the primary flame, the result agrees well with the anticipated solution that the major products of the primary flame are H_2O, NO, HCN, N_2, and CO as reported in Ref. 5. The flame temperature reaches about 1650 K. However, when the scheme is incorporated as a submodel in the complete kinetics schemes of Melius and Yetter, the resulting HCN concentration near the surface seems too high when compared with experimental observations. In addition, the gas-phase temperature increases monotonically, and there is no evidence of a temperature plateau. A detailed assessment of various chemical kinetics schemes is given in the thesis of Liau.[30]

Concluding Remarks

The combustion wave structure of RDX monopropellant has been numerically studied over a broad range of pressure. The model is based on the conservation equations of mass, energy, and species concentration in both gas and condensed phases, and includes detailed gas-phase chemical kinetics. Subsurface thermal decomposition and evaporation are also included to simulate bubble formation in the foam layer. A series of calculations was carried out to investigate the propellant burning characteristics and chemical pathways, with special attention given to the effect of the subsurface two-phase region on the flame behavior. Good agreement between experimental and predicted burning rates as well as their temperature and pressure sensitivities was achieved. The calculated species-concentration profiles suggest a multistage reaction mechanism in the gas phase. The corresponding temperature distribution, however, indicates a monotonic increase from the surface to the end of the flame zone, and no evidence was obtained showing the existence of a temperature plateau in the dark zone. In spite of the consistency of the present prediction with some experimental observations of self-sustained RDX combustion, further investigation is needed to establish a unified understanding of the flame structure under various ambient conditions.

Acknowledgments

This work was sponsored by the Army Research Office under Contract DAAL 03-92-G-0118. The support and encouragement of Robert W. Shaw is greatly appreciated. The

authors are indebted to Kenneth K. Kuo, Yeu-Cherng Lu, and Eric Boyer for helpful discussions.

References

[1]Boggs, T. L., "The Thermal Behavior of Cyclotrimethylene-trinitramine (RDX) and Cyclotetramethylene-tetranitramine (HMX)," *Fundamentals of Solid Propellant Combustion*, edited by K. K. Kuo and M. Summerfield, Vol. 90, Progress in Astronautics and Aeronautics, AIAA, New York, 1984, pp. 121–175.

[2]Fifer, R. A., "Chemistry of Nitrate Ester and Nitramine Propellants," *Fundamentals of Solid Propellant Combustion*, edited by K. K. Kuo and M. Summerfield, Vol. 90, Progress in Astronautics and Aeronautics, AIAA, New York, 1984, pp. 177–237.

[3]Alexander, M. H., Dagdigian, P. J., Jocox, M. E., Kolb, C. E., Melius, C. F., Rabitz, H., Smooke, M. D., and Tsang, W., "Nitramine Propellant Ignition and Combustion Research," *Progress in Energy and Combustion Science*, Vol. 17, No. 4, 1991, pp. 263–296.

[4]Brill, T. B., Gongwer, P. E., and Williams, G. K., "Thermal Decomposition of Energetic Materials 66. The Kinetic Compensation Effect in HMX, RDX, and NTO," *Journal of Physical Chemistry* (to be published).

[5]Korobeinichev, O. P., Kuibida, L. V., Orlov, V. N., Tereschenko, A. G., Kutsenogii, K. P., Mavliev, R. V., Ermolin, N. E., Fomin, V. M., and Emel'yanov, I. D., "Mass Spectrometric Probe Study of the Flame Structure and Kinetics of Chemical Reactions in Flames," *Mass Spectrometry and Chemical Kinetics*, 1985, pp. 73–93 (in Russian).

[6]Ermolin, N. E., Korobeinichev, O. P., Kuibida, L. V., and Formin, V. M., "Study of the Kinetics and Mechanism of Hexogen Flames," *Fizika Goreniya I Vzryva*, Vol. 22, No. 5, 1986, pp. 54–64.

[7]Zhao, X., Hintsa, E. J., and Lee, Y. T., "Infrared Multi-Photon Dissociation of RDX in a Molecular Beam," *Journal of Chemical Physics*, Vol. 88, No. 2, 1988, pp. 801–810.

[8]Melius, C. F., "Thermochemical Modeling: I & II," *Chemistry and Physics of Energetic Materials*, edited by S. N. Bulusu, Kluwer Academic, Norwell, MA, 1990, pp. 21–78.

[9]Beard, B. C., "X-Ray Radiation Decomposition of Cyclo-1,3,5-Trimethylene-2,4,6-Trinitramine (RDX) at Low Temperature: Initial Research Steps," *Propellants, Explosives, and Pyrotechnics*, Vol. 16, No. 2, 1991, pp. 81–87.

[10]Krause, H. H., Eisenreich, N., and Pfeil, A., "High Rate Decomposition of Cyclotrimethylene-trinitramine (RDX)," *Propellants, Explosives, and Pyrotechnics*, Vol. 17, 1992, pp. 179–181.

[11]Behrens, R., Jr., and Bulusu, S. N., "Thermal Decomposition of Energetic Materials 3 & 4," *Journal of Physical Chemistry*, Vol. 96, No. 22, 1992, pp. 8877–8897.

[12]Wight, C. A., and Botcher, T. R., "Thermal Decomposition of Solid RDX Begins with N-N Bond Scission," *Journal American Chemistry Society*, Vol. 114, No. 21, 1992, pp. 8303, 8304.

[13]Botcher, R. R., and Wight, C. A., "Transient Thin Film Laser Pyrolysis of RDX," *Journal of Physical Chemistry*, Vol. 97, No. 36, 1993, pp. 9149–9153.

[14]Brill, T. B., Brush, D. G., Patil, D. G., and Chen, J. K., "Chemical Pathways at a Burning Surface," *Proceedings of the 24th Symposium (International) on Combustion*, The Combustion Inst., Pittsburgh, PA, 1992, pp. 1907–1914.

[15]Fetherolf, B. L., and Litzinger, T. A., "Chemical Structure of the Gas-Phase Above Deflagrating RDX: Comparison of Experimental Measurements and Model Predictions," *Proceedings of 30th JANNAF Combustion Subcommittee Meeting*, Vol. II, CPIA Publication 606, 1993.

[16]Schroeder, M. A., "Critical Analysis of Nitramines Decomposition Data: Product Distributions from HMX and RDX Decompositions," U.S. Army Ballistic Research Lab. TR-2659, June 1985.

[17]Schroeder, M. A., "Critical Analysis of Nitramines Decomposition Data: Preliminary Comments on Autoacceleration and Autoinhibition in HMX and RDX Decompositions," U.S. Army Ballistic Res. Lab. MR-033702659, Aug. 1984.

[18]Schroeder, M. A., "Critical Analysis of Nitramines Decomposition Data: Activation Energies and Frequency Factors for HMX and RDX Decompositions," U.S. Army Ballistic Research Lab. TR-2673, Sept. 1985.

[19]Lin, C. Y., Wang, H. I., Lin, M. C., and Williams, C. F., "A Shock Tube Study of the $CH_2O + NO_2$ Reaction at High Temperature," *International Journal of Chemical Kinetics*, Vol. 22, 1990, pp. 455–482.

[20]Litzinger, T. A., Fetherolf, B. L., Lee, Y.-J., and Tang, C.-J., "Study of the Gas-Phase Chemistry of RDX: Experiments and Modeling," *Journal of Propulsion and Power*, Vol. 11, No. 4, pp. 698–703.

[21]Hanson-Parr, D., and Parr, T., "RDX Flame Structure," *Proceedings of the 25th Symposium (International) on Combustion*, The Combustion Inst., Pittsburgh, PA, 1994, pp. 1635–1643.

[22]Zenin, A., "HMX and RDX: Combustion Mechanism and Influence on Modern Double-Base Propellant Combustion," *Journal of Propulsion and Power*, Vol. 11, No. 4, 1995, pp. 752–758.

[23]Boyer, E., private communication, Pennsylvania State Univ., University Park, PA, 1995.

[24]Benreuven, M., Caveny, L. H., Vichnevetsky, R. J., and Summerfield, M., "Flame Zone and Sub-Surface Reaction Model for Deflagrating RDX," *Proceedings of the 16th Symposum (International) on Combustion*, The Combustion Inst., Pittsburgh, PA, 1976, pp. 1223–1233.

[25]Yetter, R. A., Dryer, F. L., Allen, M. T., and Gatto, J. L., "Development of Gas-Phase Reaction Mechanisms for Nitramine Combustion," *Journal of Propulsion and Power*, Vol. 11, No. 4, 1995, pp. 683–697.

[26]Li, S. C., Williams, F. A., and Margolis, S. B., "Effects of Two-Phase Flow in a Model for Nitramine Deflagration," *Combustion and Flame*, Vol. 80, Nos. 3–4, 1990, pp. 329–349.

[27]Margolis, S. B., Williams, F. A., and Armstrong, R. C., "Influences of Two-Phase Flow in the Deflagration of Homogeneous Solids," *Combustion and Flame*, Vol. 67, No. 3, 1987, pp. 249–258.

[28]Margolis, S. B., and Williams, F. A., "Influences of Porosity and Two-Phase Flow on Diffusional/Thermal Instability of a Deflagrating Energetic Material," Sandia National Lab. Rep. SAND94-8409, Nov. 1994.

[29]Margolis, S. B., and Williams, F. A., "Effects of Two-Phase Flow on the Deflagration of Porous Energetic Materials," *Journal of Propulsion and Power*, Vol. 11, No. 4, 1995, pp. 759–768.

[30]Liau, Y. C., "Numerical Analysis of RDX Monopropellant Combustion with Two-Phase Subsurface Reactions Under Steady and Transient Conditions," Ph.D. Dissertation, Pennsylvania State Univ., University Park, PA, 1996.

[31]Glarborg, P., Miller, J. A., and Kee, R. J., "Kinetic Modeling and Sensitivity Analysis of Nitrogen Oxide Formation in Well-Stirred Reactors," *Combustion and Flame*, Vol. 65, No. 2, 1986, pp. 177–202.

[32]Miller, J. A., Branch, M. C., McLean, W. J., Chandler, D. W., Smooke, M. D., and Kee, R. J., "The Conversion of HCN to NO and N_2 in H_2-O_2-HCN-Ar Flame at Low Pressure," *Proceedings of the 20th Symposium (International) on Combustion*, The Combustion Inst., Pittsburgh, PA, 1984, pp. 673–684.

[33]Thorne, L. R., Branch, M. C., Chandler, D. W., Kee, R. J., and Miller, J. A., "Hydrocarbon-Nitric Oxide Interactions in Low-Pressure Flames," *Proceedings of the 21st Symposium (International) on Combustion*, The Combustion Inst., Pittsburgh, PA, 1986, pp. 965–977.

[34]Scheidegger, A. E., *The Physics of Flow Through Porous Media*, 3rd ed., Univ. of Toronto Press, Buffalo, NY, 1974.

[35]Brill, T. B., "Multiphase Chemistry Considerations at the Surface of Burning Nitramine Monopropellants," *Journal of Propulsion and Power*, Vol. 11, No. 4, 1995, pp. 740–751.

[36]Thynell, S. T., Gongwer, P. E., and Brill, T. B., "Modeling of Thermal Response of Filament Used in T-Jump Experiments," *Proceedings of the 31st JANNAF Combustion Subcommittee Meeting*, CPIA Publication, 1994.

[37]Kee, R. J., Grcar, J. F., Smooke, M. D., and Miller, J. A., "A Fortran Program for Modeling Steady, Laminar, One-Dimensional, Premixed Flames," Sandia National Lab. Rep. SAND85-8240, Dec. 1985.

[38]Gibbs, T. R., and Popolato, A., *LASL Explosive Property Data*, Univ. of California Press, Berkeley, CA, 1980, pp. 141–151.

[39]Kubota, N., "Survey of Rocket Propellants and Their Combustion Characteristics," *Fundamentals of Solid Propellant Combustion*, edited by K. K. Kuo and M. Summerfield, Vol. 90, Progress in Astronautics and Aeronautics, AIAA, New York, 1984, pp. 1–52.

[40]Li, S. C., and Williams, F. A., "Nitramine Deflagration: A Reduced Chemical Mechanism for the Primary Flame," AIAA Paper 94-3041, June 1994.

[41]Zimmer-Galler, R., "Correlations Between Deflagration Characteristics and Surface Properties of Nitramine-Based Propellants," *AIAA Journal*, Vol. 6, No. 11, 1968, pp. 2107–2110.

[42]Glaskov, A. P., "The Effect of Catalysts on the Combustion of Explosives," *Fizika Goreniya i Vzryva*, Vol. 10, No. 3, 1974, pp. 323–334.